ARTICLES
PUBLISHED ONLINE: 24 NOVEMBER 2014 | DOI: 10.1038/NPHOTON.2014.278
nature photonics

Measuring the temporal structure of few-femtosecond free-electron laser X-ray pulses directly in the time domain

W. Helml[1,2†], A. R. Maier[3,4†], W. Schweinberger[2], I. Grguraš[3,5], P. Radcliffe[6], G. Doumy[7,8], C. Roedig[8], J. Gagnon[2], M. Messerschmidt[9], S. Schorb[9], C. Bostedt[9], F. Grüner[3,4], L. F. DiMauro[8], D. Cubaynes[10], J. D. Bozek[9], Th. Tschentscher[6], J. T. Costello[11], M. Meyer[6,10], R. Coffee[9], S. Düsterer[12], A. L. Cavalieri[3,5] and R. Kienberger[1,2*]

Short-wavelength free-electron lasers are now well established as essential and unrivalled sources of ultrabright coherent X-ray radiation. One of the key characteristics of these intense X-ray pulses is their expected few-femtosecond duration. No measurement has succeeded so far in directly determining the temporal structure or even the duration of these ultrashort pulses in the few-femtosecond range. Here, by deploying the so-called streaking spectroscopy technique at the Linac Coherent Light Source, we demonstrate a non-invasive scheme for temporal characterization of X-ray pulses with sub-femtosecond resolution. This method is independent of photon energy, decoupled from machine parameters, and provides an upper bound on the X-ray pulse duration. We measured the duration of the shortest X-ray pulses currently available to be on average no longer than 4.4 fs. Analysing the pulse substructure indicates a small percentage of the free-electron laser pulses consisting of individual high-intensity spikes to be on the order of hundreds of attoseconds.

Since the first discovery of X-rays as a means for the measurement of crystal structures[1], three-dimensional imaging techniques with X-rays for the investigation of the spatial composition of crystalline materials and biological specimens have steadily been refined to reach their current nanoscale resolution. With the advent of free-electron lasers[2–5] (FELs) operating on the self-amplified spontaneous emission—SASE—principle[6], sources of high-intensity femtosecond X-ray pulses are now available. Combining high spatial resolution and ultrashort duration, these pulses open the door to full four-dimensional 'movies' that convey simultaneous information on atomic structure and function. The implementation of these femtosecond X-ray pulses as a reliable tool for four-dimensional characterization with ultrafast temporal and atomic spatial resolution, as demonstrated by some pioneering experiments with synchrotron radiation[7] or electrons[8,9], requires exact knowledge of the duration and temporal structure of individual X-ray pulses in the interaction region. Generally, this is not just a crucial requirement for time-resolved measurements[10,11]; the precise assessment of peak intensities also forms the fundamental basis for any nonlinear studies[12,13] as well as successful single-shot diffraction experiments on non-repetitive and non-reproducible structures, like those demonstrated with individual biomolecules, membrane proteins or viruses[14–16].

Modern SASE FELs are able to produce coherent extreme ultraviolet (XUV)[17,18] and X-ray[5,19] radiation with sufficient intensities for single-shot or pump–probe measurements. The Linac Coherent Light Source[5] (LCLS) has the additional advantage of being easily tuned in photon energy as well as in average pulse duration. For our investigations of the shortest possible X-ray pulses, the LCLS was working in the so-called 'low-charge mode', producing X-ray pulses expected to be of sub-10 fs duration[20]. Due to the SASE process, the underlying temporal structure of the emitted pulses is stochastic, which means that each subsequent X-ray pulse is inherently different from the last one[21]. In addition, FEL pulses suffer from intrinsic timing jitter introduced by the electron accelerator with respect to a measurement device in the lab frame. As a consequence, a single-shot measurement is required for the determination of the time structure of consecutive SASE X-ray pulses.

The X-ray pulse duration can be indirectly inferred from measurements on the electron bunch length before stimulated emission of X-ray Bremsstrahlung in the undulator. Although this method is capable of resolving electron bunch lengths as short as 25 fs (ref. 5), studies of fundamental ionization processes and recent two-colour cross-correlation measurements on longer X-ray pulses (>40 fs) have revealed a substantial deviation of the actual X-ray pulse duration from the measured electron bunch length[12,22]. Another cutting-edge approach involves measuring the time-resolved electron beam energy loss and energy spread induced by the FEL process, with a transverse radiofrequency deflector located after the undulator[23]. However, all these measurements

[1]Technische Universität München, Physik-Department E11, James-Franck-Straße, 85748 Garching, Germany, [2]Max-Planck-Institut für Quantenoptik, Hans-Kopfermann-Straße 1, 85748 Garching, Germany, [3]Center for Free-Electron Laser Science (CFEL), Notkestraße 85, 22607 Hamburg, Germany, [4]Institut für Experimentalphysik, Gruppe Beschleunigerphysik, University of Hamburg and Center for X-ray Free-Electron Laser Science, Luruper Chaussee 149, 22761 Hamburg, Germany, [5]Max-Planck Institute for the Structure and Dynamics of Matter, Luruper Chaussee 149, 22761 Hamburg, Germany, [6]European XFEL, Albert-Einstein-Ring 19, 22761 Hamburg, Germany, [7]Argonne National Laboratory, Argonne, Illinois 60439, USA, [8]Department of Physics, The Ohio State University, Columbus, Ohio 43210, USA, [9]Linac Coherent Light Source, 2575 Sand Hill Road, Menlo Park, California 94025, USA, [10]Institut des Sciences Moléculaires d'Orsay, UMR 8214, CNRS–Université Paris Sud, Bâtiment 350, 91405 Orsay Cedex, France, [11]School of Physical Sciences and National Center for Plasma Science and Technology (NCPST), Dublin City University, Glasnevin, Dublin 9, Ireland, [12]DESY, Notkestraße 85, 22607 Hamburg, Germany; †These authors contributed equally to this work. *e-mail: reinhard.kienberger@tum.de

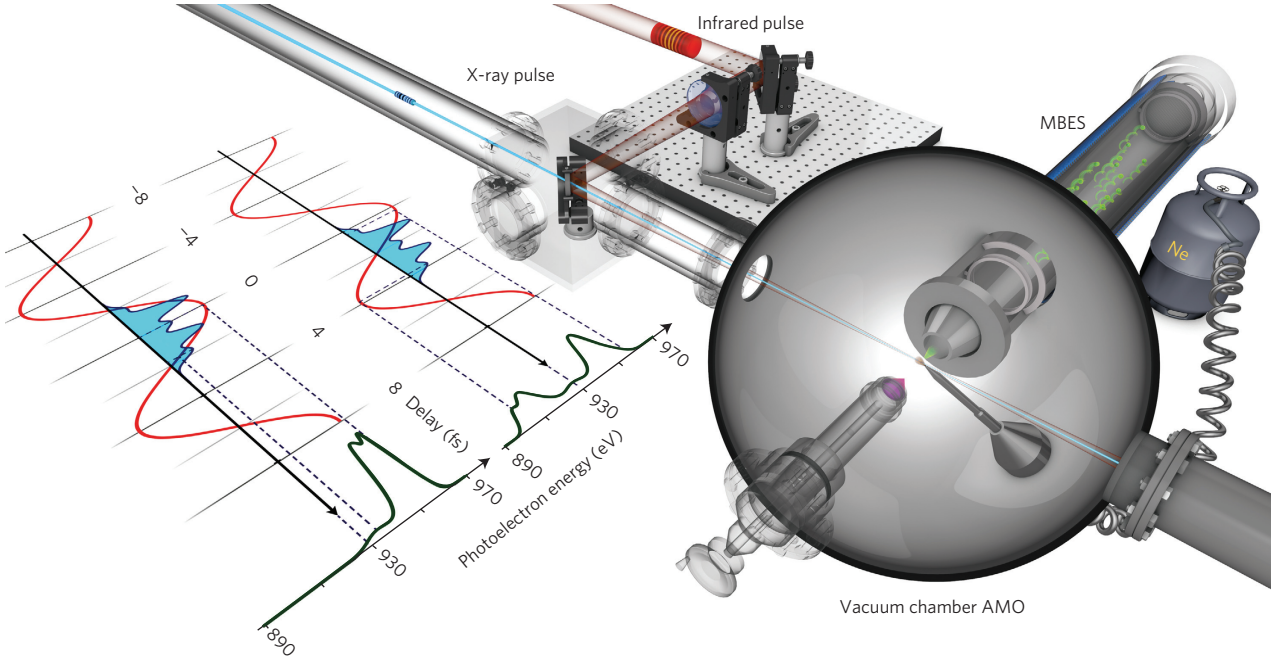

Figure 1 | Experimental set-up and measurement principle at the LCLS. Experimental set-up in the AMO hutch at the LCLS. The X-ray laser and NIR streaking laser are coupled into the vacuum chamber and are co-linearly focused onto a Ne gas target. The generated photoelectrons are then energy-resolved with a magnetic bottle electron spectrometer. The inset on the left depicts two distinctive cases of temporal overlap of the FEL with respect to the streaking field, one at the zero-crossing and one at a maximum of the NIR vector potential. The respective photoelectron spectra are also shown. More details are given in the text.

provide only indirect evidence, as they are working on the generating electron bunch instead of the X-ray pulse itself. To date, no direct experimental determination of the temporal structure of few-femtosecond SASE X-ray pulses has yet been feasible, due to their X-ray nature, ultrashort duration and the inherent jitter in their arrival time. This situation is also substantially different in comparison to earlier measurements on longer X-ray pulses[22,24] or FEL pulses with lower photon energies[25].

NIR streaking spectroscopy of FEL pulses

To directly measure the FEL pulse duration we rely on the method of near-infrared (NIR) streaking spectroscopy[26,27], a well-established technique for temporal characterization of attosecond pulses in the XUV spectral region[28]. In this approach, an NIR laser field that is coarsely synchronized to the X-ray pulse is spatially overlapped with the X-ray beam in a dilute gas target. Here, Ne gas atoms are ionized by the FEL and the generated photoelectrons are detected with a magnetic bottle electron spectrometer[29] (MBES). With an FEL photon energy of $E_\gamma \approx 1{,}791$ eV and a binding energy of $E_B \approx 870$ eV for the 1*s* electron shell in Ne, the kinetic energy of the photoelectrons in the absence of the NIR laser is distributed around a mean value of ~921 eV. Thus, each photoelectron can be modelled as a free wave packet, and the temporal structure of the complete photoelectron burst is a replica of the incoming FEL pulse[30]. An in-depth description of the experimental set-up is given in the Methods, and more details are provided in the Supplementary Methods.

Figure 1 presents the experimental set-up and illustrates the basic principle of streaking. Photoelectron spectra generated in the presence of an external optical laser field are called 'dressed' spectra. These dressed photoelectron spectra exhibit specific characteristics that depend (among other parameters) strongly on the duration of the cycle period of the dressing laser field t_{period}, with respect to the duration of the FEL pulses, $\tau_{\mathrm{X\text{-}ray}}$, to be measured.

In general, one can discern two distinct cases of dressed photoelectron spectra, defined by the ratio of the dressing field period to the duration of the X-ray pulses that generate the photoelectrons (cf. ref. 31). For periods of the dressing field shorter than the X-ray pulse duration ($t_{\mathrm{period}}/\tau_{\mathrm{X\text{-}ray}} < 1$), measurements belong to the 'sideband regime', which is characterized by the appearance of new photolines, symmetrically distributed on both sides of the original undressed line and spaced by an energy that corresponds to the optical frequency of the applied dressing field (see, for example, refs 22, 32 and 33). In this case the photoelectron spectra are sensitive to the contributions of more than one optical period and accordingly depend on the cycle-averaged intensity envelope of the dressing laser.

When the duration of the X-ray pulses is shorter than the period of the dressing field ($t_{\mathrm{period}}/\tau_{\mathrm{X\text{-}ray}} > 1$), the photoelectron spectra are dressed in the so-called 'streaking regime'. Because the X-ray pulse only extends over a part of the period of the dressing field, the photoelectrons generated at different delays between the FEL and the NIR pulse experience a redistribution in energy that depends on the magnitude of the electric field at the instant of their generation. In this way, the electron spectra are significantly changed in their final energy spread and central energy with respect to the unstreaked photoelectron burst (Fig. 1, left). In our conditions, the overall shift $\Delta\varepsilon$ of the central energy of the photoelectron spectrum at an extremum of the streaking vector potential can be approximated using the classical formula[26,34]

$$\Delta\varepsilon(t_b) \approx -p_c A_{IR}(t_b) \quad (1)$$

where p_c is the momentum corresponding to the central energy ε_c of the unstreaked photoelectrons via $p_c = \sqrt{2\varepsilon_c}$ (in atomic units, a.u.: $\hbar = e = m_e = \frac{1}{4\pi\varepsilon_0} = 1$). $A_{IR}(t_b)$ is the vector potential of the streaking field at the moment of birth of the electron wave packet (t_b) and is related to the electric field by $E_{IR}(t) = -\mathrm{d}A_{IR}(t)/\mathrm{d}t$.

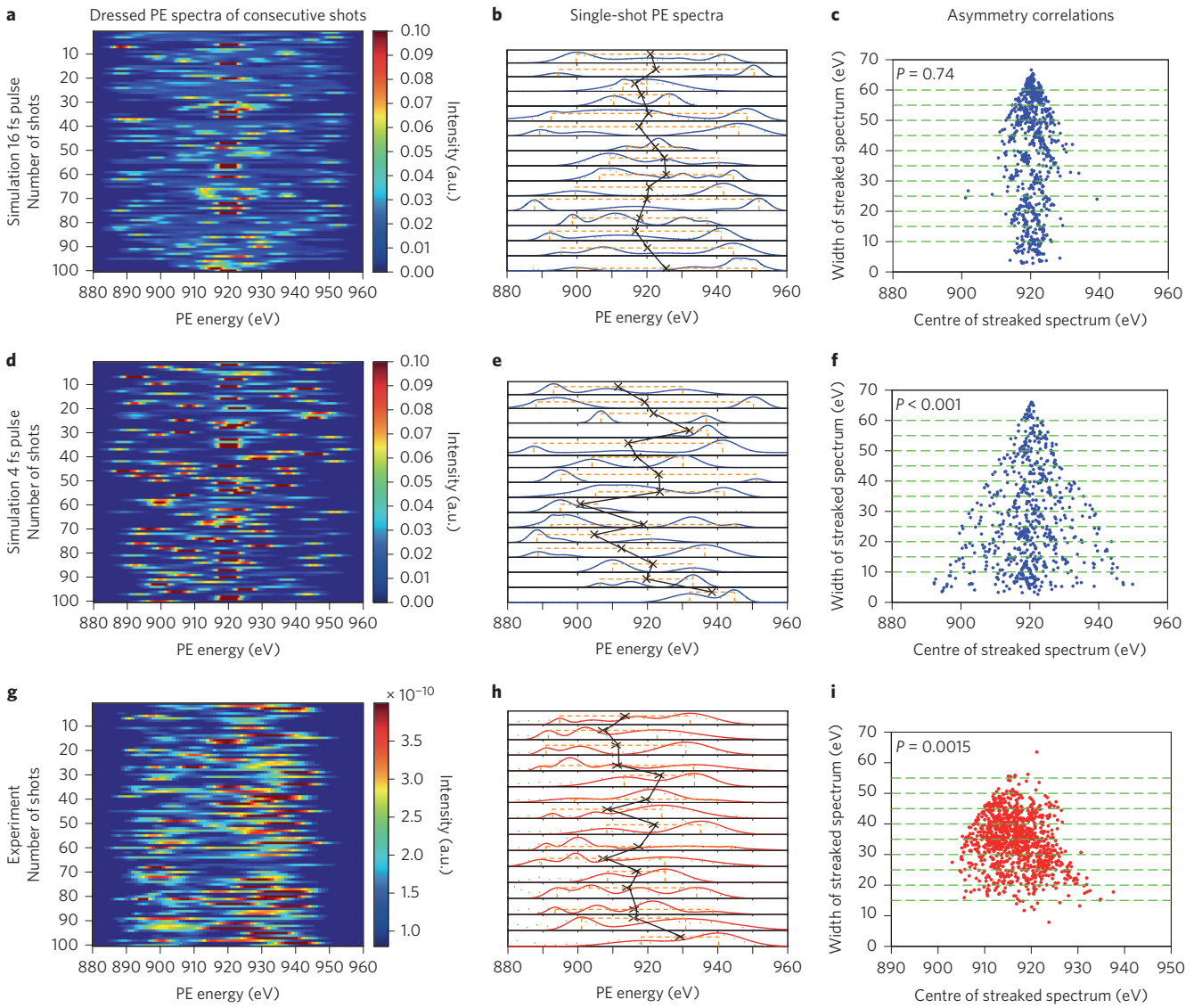

Figure 2 | Dressed single-shot X-ray photoelectron spectra and correlation plots. a–i, Simulations (blue, **a–c**, **d–f**) for the sideband regime with 16 fs FEL pulses ($t_{period}/t_{X\text{-}ray} = 1/2$, **a–c**) and for the streaking regime with 4 fs FEL pulses ($t_{period}/t_{X\text{-}ray} = 2$, **d–f**) are compared with experimental findings (**g–i**, red). On the left (**a**,**d**,**g**), colour-coded intensity images of 100 consecutive dressed photoelectron (PE) spectra are plotted. In the middle (**b**,**e**,**h**), 15 single-shot spectra are extracted for the three cases. For each, the spectral width (orange, dashed lines) and centre position (black crosses) are marked, with black lines connecting the centres of consecutive spectra. On the right, the centre positions and widths of the spectra for 1,000 simulated shots (**c**,**f**) and for the experimental data (**i**) are mapped out in correlation scatter plots.

Photoelectron dressing in the streaking regime is illustrated in the inset in Fig. 1. When the generation of the photoelectrons by the X-ray pulse coincides with a zero-crossing of the vector potential of the streaking laser, the finite X-ray pulse duration ensures that electrons are born to either side of the zero-crossing and the photoelectron spectrum is symmetrically broadened around the central undressed photoline; however, the spectrum is either upshifted or downshifted in energy when the photoelectrons overlap with an extremum of the vector potential, in accordance with equation (1). Therefore, in a single-shot measurement, one can observe the appearance of asymmetry in the dressed photoelectron spectra depending on the exact moment of ionization with respect to the electric field of the streaking laser. Thus, the temporal profile of the X-ray pulse is mapped onto the energy domain and is made directly accessible via electron spectroscopic measurements[30,34].

To ensure an unambiguous mapping of a given electron birth time to a detected final energy, it is crucial to determine a measure for the X-ray pulse duration compared to the streaking laser period. Following the previous reasoning, this can be achieved by making use of the spectral asymmetry that is introduced solely when working in the streaking regime and is therefore a uniquely identifying feature for this case. Figure 2 shows how we can obtain such a quantitative measure for the ratio of the X-ray pulse length $\tau_{X\text{-}ray}$ with respect to the streaking laser period ($t_{period} = 8$ fs) from our data. The figure presents two simulated cases in the first two rows, one for the sideband regime with 16 fs FEL pulses ($t_{period}/\tau_{X\text{-}ray} = 1/2$, Fig. 2a–c) and one for the streaking regime with 4 fs FEL pulses ($t_{period}/\tau_{X\text{-}ray} = 2$, Fig. 2d–f). These simulations are compared with our experimental findings, which are presented in the third row (Fig. 2g–i).

There is a distinct correlation of the spread of the central energies with the spectral widths for the simulation of streaked spectra for 4 fs FEL pulses (Fig. 2f). The wider the spectra, the smaller the spread of the centres of the spectra around the value of the unstreaked photoline. This dependency is only discernible for dressed spectra with pulse durations $\tau_{X\text{-}ray} < t_{period}$ and completely vanishes for

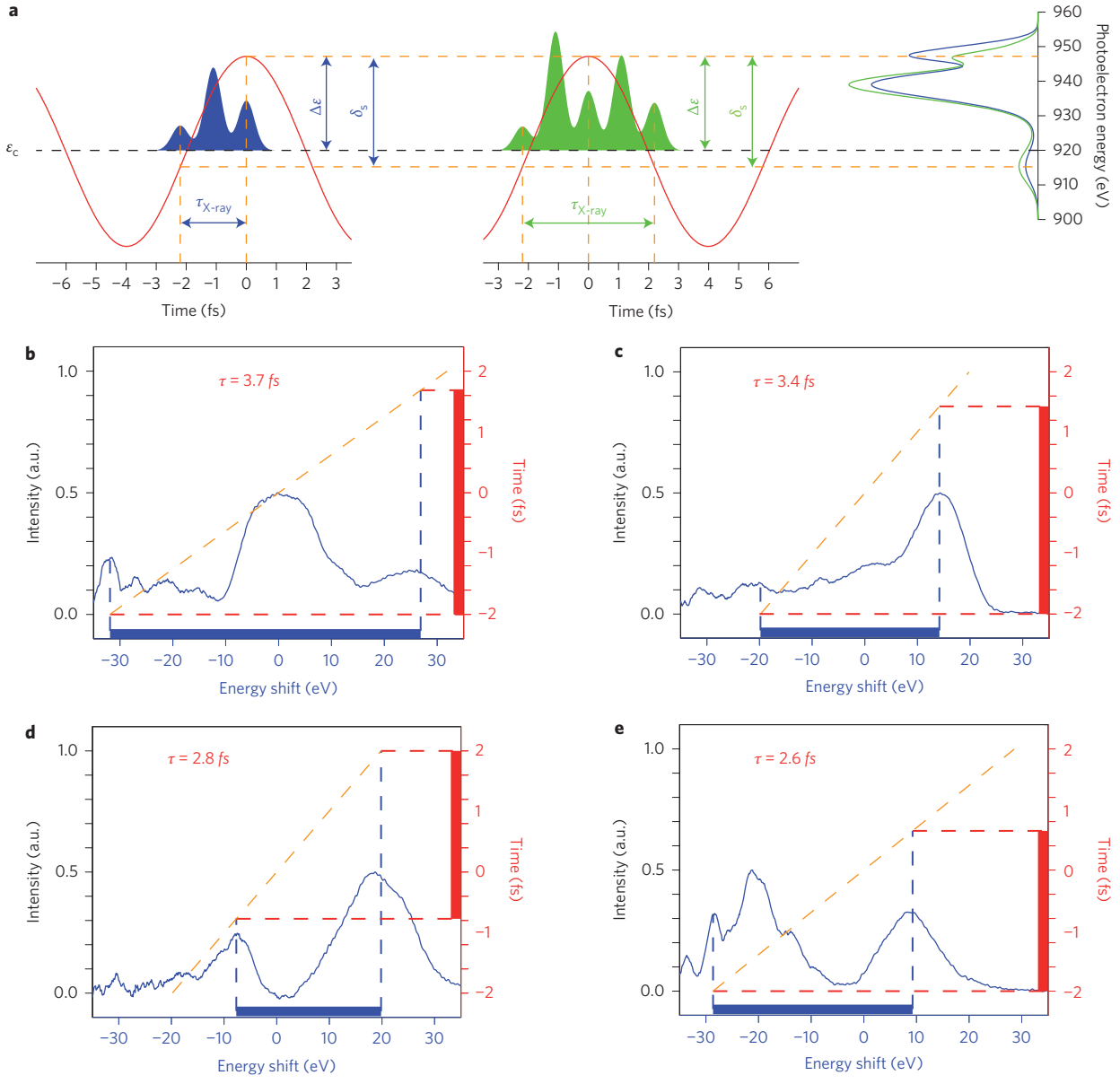

Figure 3 | Streaking of few-femtosecond X-ray pulses. a, Principle of X-ray pulse duration evaluation. **b**–**e**, Four different streaked photoelectron spectra as measured in our experiment (blue solid lines) at different values of the NIR vector potential, and the respective linear streaking ramps (orange dashed lines) derived from the maximum shifted peak of each spectrum. In **b**, the streaked spectrum spans from −32 eV to 27 eV; that is, the NIR laser quarter-cycle of 2 fs is mapped onto the maximum shift of |−32| eV and the complete spectral width of 59 eV therefore corresponds to a pulse duration upper limit of 3.7 fs (all pulse durations are FWHM). In a similar manner we derive pulse duration upper limits of 3.4 fs (**c**), 2.8 fs (**d**) and 2.6 fs (**e**). Considering the ambiguity of the energy-to-time mapping, all those shots are in principle also compatible with the doubled pulse lengths.

X-ray pulses that are longer than the NIR cycle period, as for the 16 fs FEL pulses in Fig. 2c. This correlation therefore defines an unambiguous feature of single-shot spectra obtained in the streaking regime. When comparing with our experimental data (Fig. 2i), we see a clear correlation resembling the spectra simulated with the 4 fs X-ray pulses. Calculating the statistical significance of these correlations confirms this qualitative conclusion: the correlation for the simulated case of the 16 fs X-ray pulses turns out not to be significant ($P \gg 0.05$), while the correlations for the simulations of spectra from 4 fs FEL pulses ($P < 0.001$) and the experimental results ($P = 0.0015$) are easily in the range of the limit for statistical significance. We have thereby shown, qualitatively and quantitatively, that our measurements are conducted in the streaking regime and thus that the associated pulse retrieval methods are valid. Details concerning the applied streaking simulations, the calculation of the correlation matrix and more correlation plots that corroborate these conclusions are provided in Supplementary Methods.

Temporal structure of few-femtosecond X-ray pulses

Because the time jitter between FEL and NIR pulses is of the same order as the NIR pulse duration[35], it is not possible to control the delay of the NIR with respect to each single FEL pulse. As the relative delay between the X-ray pulse and the streaking field is not known *a priori*, we must first determine the actual value of the vector potential for each individual FEL pulse. In a second step we use this vector potential as a calibration factor to convert the measured spectral width of each streaked photoelectron burst into the duration of the corresponding X-ray pulse.

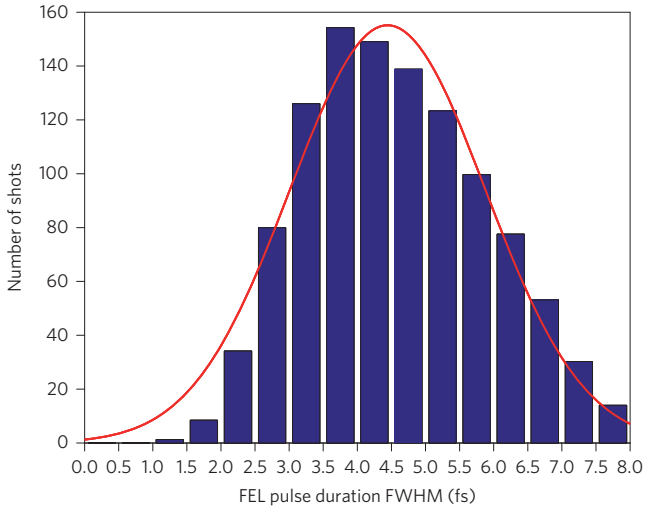

Figure 4 | Average FEL pulse duration upper limit. Histogram of all possible pulse duration upper limits in agreement with our measurement for each shot (blue), for the parameter range used at LCLS (20 pC low-charge mode, 1,791 eV X-ray photon energy, electron bunch near full compression at 10 kA, slotted foil inserted into the electron beam path). The red solid line shows a Gaussian fit to the distribution, indicating an average X-ray pulse duration upper limit of ~4.4 fs FWHM.

The evaluation principle for the X-ray pulse duration is depicted in Fig. 3a and described in detail in the Methods. In short, the maximal shifted peak of the measured photoelectron spectrum is associated with an overlap of the X-ray pulse with a local extremum of the streaking field (compare the blue pulse on the left in Fig. 3a). This energy shift $\Delta\varepsilon$ defines the gradient of the energy-to-time conversion, and the overall width δ_s of the streaked spectrum is used for the determination of the FEL pulse duration.

In the simulated example in Fig. 3a the streaked spectrum ranges from 915 to 945 eV, corresponding to a width of $\delta_s = 30$ eV and a maximal shifted peak at 945 eV of $\Delta\varepsilon = 945–920 = 25$ eV with respect to the unstreaked photoline at 920 eV. Following ref. 34, we estimate the vector potential A_{IR} using

$$A_{IR} \approx -E_{peak} \times (t - t_{peak}) \quad (2)$$

which assumes that the streaking field is approximately linear in time, with a slope given by the peak electric field $E_{peak} = E(t_{peak})$ of the half-cycle with which the photoelectrons are overlapping. The cycle period of our streaking laser was $t_{period} = 8$ fs, setting the time interval for the vector potential to rise from a zero-crossing to an extremum (a quarter period) as $8/4 = 2$ fs. This interval corresponds to the above-calculated maximum shift $\Delta\varepsilon = 25$ eV in the energy domain. Now we can use the total width of the streaked spectrum, $\delta_s = 30$ eV, as a ruler for the pulse length, resulting in a measure for an upper limit of the full-width at half-maximum (FWHM) X-ray pulse duration:

$$\tau_{X\text{-ray}} = \frac{\delta_s}{\Delta\varepsilon} \times \frac{t_{period}}{4} \quad (3)$$

This gives $(30/25) \times 8/4 = 2.4$ fs in our simulated case, fitting the blue X-ray pulse on the left in Fig. 3a.

The green X-ray pulse, which is twice as long (as depicted in the middle of Fig. 3a), gives rise to a very similar PE spectrum, leading to a residual ambiguity of the FEL pulse length measurement. In this case, the pulse length upper limits between 2.4 fs and 4.8 fs are all compatible with the simulated streaking spectrum.

Owing to the statistical nature of the SASE-generated FEL pulses originating from noise, the X-ray pulse profile differs greatly from shot to shot. For the first time we are able to show this variation and reveal the intensity substructure of few-femtosecond FEL pulses directly in the time domain, with a resolution better than the coherence length[21]. Figure 3b–e shows examples of four different measured single-shot photoelectron spectra (blue traces) and the derived pulse duration upper limits of the generating X-ray pulses (in red on the right vertical axes). In Fig. 3b, an FEL pulse consisting mainly of one central peak overlaps with the zero-crossing of the vector potential, and its photoelectron spectrum is therefore uniformly broadened. In contrast, different arrival times of the FEL pulse relative to the streaking laser lead to an overall shift of the whole spectrum, as depicted in Fig. 3d,e, where the FEL pulse mostly overlaps with the positive or negative part of the vector potential, respectively, and the resulting spectrum is shifted accordingly. An individual peak with an extended single-sided shoulder (Fig. 3c) can be distinguished from a pulse containing two well-separated spikes (Fig. 3d) or even a whole train of individual spikes as shown in Fig. 3e.

If we repeat this analysis for all shots and plot the results as a histogram, summing over the respective pulse duration upper limits with which each single X-ray pulse is compatible (from 2.4 fs to 4.8 fs in the case of the shot from Fig. 3a, for example), we obtain an estimate of the average X-ray pulse duration limit (Fig. 4). We find that the average pulse duration upper bound of the FEL in our mode of operation is best fit by a Gaussian distribution (red curve) with a mean value of ~4.4 fs FWHM.

Coherent sub-femtosecond X-ray spikes

Due to pulse-to-pulse fluctuations, some pulses are considerably shorter than the average duration. FEL theory predicts a temporal pulse substructure composed of a train of ultrashort intensity spikes[21] with a typical duration corresponding to the coherence time. In our conditions, single spikes of ~1 fs and below are expected (compare, for example, ref. 20). The number of spikes per pulse is subject to shot-to-shot variations and occasionally an X-ray pulse consisting of only one isolated spike is generated. A single spike pulse implies full temporal coherence, a remarkable feature usually absent in FEL pulses. Close examination of our data confirmed the existence of such ultrashort 'single-spike' pulses, constituting about 5% of all shots.

The analysis procedure described above is partially compromised for single-spike pulses by the arrival time jitter. It is not applicable in the cases when the X-ray pulse in reality coincides with an extremum of the vector potential, because at these points the linear ramp approximation given in equation (2) for the streaking field breaks down (see Supplementary Discussion section 'Evaluation of single-spike X-ray pulses' for a more elaborate discussion). Accordingly, although we cannot deduce the exact pulse duration for any one specific shot, the method provides a correct upper limit in most cases and allows us to derive a 'typical' duration range for these fully coherent single-spike X-ray pulses.

Figure 5 shows the measurement principle for attosecond X-ray pulses on the basis of one example selected from our data, marked as the larger light blue dot in the scatter plot in Fig. 5b. In the upper-right quadrant of Fig. 5a, the measured spectrum and a Gaussian fit for this shot are plotted as the dark blue full and red dashed lines, respectively. The feature centred at 905 eV in the measured spectrum might be an artefact produced by the detector electronics or a temporally well-separated small satellite pulse that is ignored for the purpose of this single-spike analysis. Comparing with the unstreaked photoline (green dotted line), the energy shift amounts to $\Delta E = 15.3$ eV. This value determines the slope of the linear ramp for the conversion from energy to time and, following deconvolution of the initial unstreaked X-ray photon energy bandwidth,

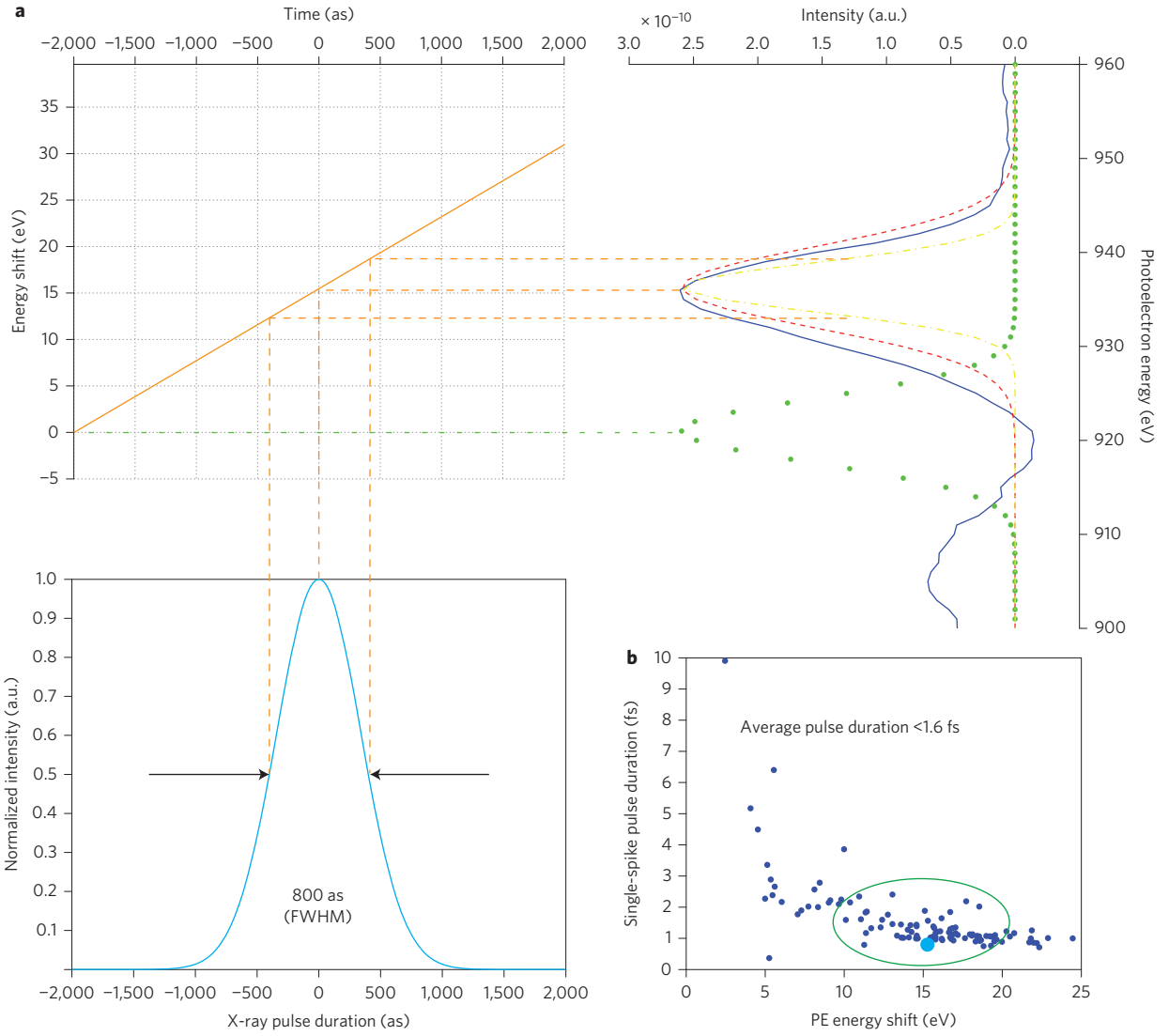

Figure 5 | Measurement of an attosecond FEL X-ray pulse. a, Measured spectrum (right) of a single FEL intensity spike (solid dark blue line) and the corresponding Gaussian fit (dashed red line). The shift of the peak from the unstreaked central energy at ~921 eV (green dotted line) defines the energy-to-time ramp (left), with the help of which the width of the deconvoluted spectrum (yellow dashed-dotted line) can be converted into a measure for the pulse duration upper limit, depicted as the light blue curve (bottom left). **b**, Derived upper limits for the pulse durations of all single-spike shots as a function of the energy shift of the peak. The pulse described in **a** is marked as the bigger light blue dot. Most of the shots with an energy shift between 10 eV and 20 eV are in the region of 1.6 fs FWHM and below (indicated by the green oval in **b**).

the measured signal is consistent with an X-ray pulse with a duration of maximum ~800 as (FWHM). For streaking spectra with a high likelihood of being generated by the linear part of the vector potential (as described in Supplementary Discussion section 'Applicability of the 'linear ramp approximation'), the derived upper limits for the duration of fully coherent X-ray single-spike pulses are mainly in the range from 750 as to 1,500 as (FWHM; marked by the green oval in Fig. 5b), which is in good agreement with the predictions based on equations for the SASE process under the conditions of the LCLS machine parameters[20].

Discussion

In conclusion, we have experimentally demonstrated that the FEL X-ray source at LCLS is capable of producing high-energy, ultra-bright pulses with an average duration of only a few femtoseconds. Our method of streaking spectroscopy allows us, for the first time, to conduct consecutive single-shot measurements of these ultra-short X-ray pulses directly in the time domain with sub-femto-second resolution and independent of the photon energy. We determined upper limits for the duration of these X-ray FEL pulses and showed that a statistical evaluation yields a characteriz-ation of the average pulse duration upper bound for a given setting of the machine parameters of the FEL. In addition, we were able to investigate the stochastic substructure of these pulses and confirmed the expected behaviour of an underlying train of ultrashort, high-intensity spikes for the SASE FEL pulses.

These spikes have the unique property of being ultrashort and fully coherent bursts of extremely intense X-ray radiation. The ability to detect and characterize FEL shots that contain only one single coherent spike makes them perfect candidates for ultrafast pump–probe experiments and all kinds of intensity-dependent studies in the soft and hard X-ray wavelength range, where a well-behaved temporal profile and coherence are highly desirable. The duration of these single-spike X-ray pulses was measured to be on the order of hundreds of attoseconds, in good agreement with theoretical predictions.

The set-up as described above only requires a fraction of the available FEL power, which can be adjusted via the gas density in

the interaction region, and is therefore suitable as a real-time diagnostic that can be used online and in parallel with an active experiment. Although the current measurement was restricted by the limitations imposed by the timing jitter between the FEL and the NIR laser, future use of a streaking source with a suitably long wavelength in the range of 10 μm will overcome the residual ambiguity. Hence, streaking spectroscopy is an ideal technique for tagging the duration of each subsequent FEL pulse during an ongoing measurement, with the potential of providing complete information on the X-ray pulse structure. This would enable the development of a versatile, ultrabright X-ray instrument with tunable photon energies and custom-tailored pulse characteristics for the investigation of inorganic materials, biological systems and molecular reaction dynamics with nanoscale spatial and attoscale temporal resolution.

Methods

Experimental set-up. We performed the measurements at the atomic, molecular and optical science (AMO) instrumental end-station at the LCLS[36]. This comprises a vacuum chamber inside which an optical laser co-propagates with the FEL. Both beams are focused into the same interaction region where a nozzle emits a jet of Ne gas. In addition, the instrumentation incorporates a MBES[29], a high-collection-efficiency spectrometer that operates over a broad energy range capable of detecting the photoelectron spectra for every single shot. For our investigations of the shortest possible X-ray pulses, the LCLS was working in the so-called 'low-charge mode', producing X-ray pulses expected to be of sub-10 fs duration[20]. To further minimize the FEL pulse duration, a 'slotted spoiler'[37] was inserted into the electron beam before the X-ray generation in the undulator. Coupling into the FEL vacuum beamline was accomplished by passing the beam through a CaF_2 window glued to a flange cut at Brewster's angle to minimize reflective losses, and reflection off a mirror (mounted at 45° with respect to the X-ray propagation direction) with a hole in the middle, through which the FEL beam passed. As a target for photoexcitation we used Ne gas streaming from a nozzle with a background pressure in the experimental chamber of $\sim 1 \times 10^{-7}$ mbar.

Parameters for the streaking laser. The streaking laser was based on an optical parametric amplifier (TOPAS-C, Light Conversion). We used the idler wave tuned to 2.4 μm central wavelength, with horizontal polarization of the electric field, a pulse energy of ~30 μJ and a compressed pulse duration of ~50 fs, measured as FWHM by a custom-built second-order autocorrelator. The output beam of the NIR laser was suitably enlarged by a telescope, then transported to the experimental chamber by reflection on silver mirrors and subsequently focused through a 2-inch CaF_2 lens to a beam diameter of ~450 μm in the interaction region, yielding an optical intensity on target of $\sim 4 \times 10^{11}$ W cm^{-2}. From this and from the maximum detected photoelectron shifts, we estimated the corresponding peak vector potential of the streaking field to be in the range $A_{peak} \approx 0.15$–0.17 a.u.

FEL settings. The LCLS was working at a repetition rate of 60 Hz in the 'low-charge mode', with an electron bunch charge of 20 pC around the point of maximum compression at ~10 kA, producing FEL pulses expected to be of sub-10 fs duration, dependent on the photon energy, which was tunable from 800 to 2,000 eV for the AMO instrumental end station[5]. FEL theory predicts a temporal pulse substructure composed of a train of ultrashort intensity spikes[21] with a typical width corresponding to the coherence time, characterized by the X-ray photon energy bandwidth. A slotted spoiler[37] was inserted into the electron beam at the second bunch-compressor chicane along the SLAC Linac ahead of X-ray generation in the undulator. We measured various characteristics of the FEL. Slight X-ray central energy variation from shot to shot is manifested as a small energy jitter of <1 eV root mean square (r.m.s.) of the photoline peak at ~921 eV, as we detected with the MBES. The bandwidth of the photoline, corresponding to the energy spread of the X-ray pulse, was measured to be ~3.4 eV (r.m.s.).

Streaking evaluation. The overall shift $\Delta\varepsilon$ of the central energy of the photoelectron spectrum at an extremum of the streaking vector potential can be described according to the classical formula[26,34] $\Delta\varepsilon(t_b) \approx -p_c A_{IR}(t_b) + \frac{1}{2}A_{IR}^2(t_b)$. The second term in this equation, the ponderomotive shift $U_p \propto A_{IR}^2$, is negligible for the streaking intensity used in our measurement, so $\Delta\varepsilon$ is directly proportional to A_{IR} and hence to the temporal integral of the electric field.

The evaluation principle for the X-ray pulse duration is illustrated in Fig. 3a. We simulated the temporal overlap of the NIR field (in red) with the FEL for two cases of X-ray pulses with different durations (blue and green), and calculated the respective streaked photoelectron spectra (on the right). First we take a look at the blue photoelectron spectrum generated by the shorter X-ray pulse. To determine the actual NIR field strength corresponding to a given FEL shot, each streaked PE spectrum is deconstructed into a number of Gaussian sub-peaks. For every spectrum the peak with the biggest shift from the unstreaked energy is identified as stemming from an overlap of the X-ray pulse with a local extremum of the streaking vector potential. This way, we assume the smallest possible slope of the vector potential that is in agreement with the measured spectrum for this shot, defining a lower bound for the effective streaking strength. Thus, a self-calibrated conversion factor from the energy to the time domain is deduced for each individual FEL shot, allowing us to derive a corresponding upper limit for the X-ray pulse duration.

There is, in addition, a residual ambiguity in the analysis method due to the timing jitter between the FEL and the NIR laser that we need to consider. Figure 3a shows schematically a second FEL pulse (green, middle) with a different duration that nevertheless leads to nearly the same measured width of the streaked spectrum. This ambiguity arises from the assumption that the X-ray pulse partly overlaps with a local extremum of the streaking vector potential, which we made to determine its instantaneous value for each shot. Because we cannot discern streaking effects caused by the rising (left) or the falling (right) edge of this vector potential curve, both could contribute to the energy spread of the detected spectrum. To obtain a correct upper limit for the possible X-ray pulse duration, we must therefore double the above-calculated value to 4.8 fs. All pulse length upper limits between 2.4 fs and 4.8 fs are compatible with this simulated measurement. We want to stress that in Fig. 4 we plot single-shot pulse duration upper limits, taking into account also the ambiguity that is introduced by the random arrival time jitter between the streaking laser and the X-ray pulses. The deduced mean value for the pulse duration is therefore a (very conservative) upper limit. A step-by-step description of the signal evaluation routine is also given in Supplementary section 'Discussion'.

Received 31 October 2013; accepted 14 October 2014; published online 24 November 2014

References

1. Friedrich, W., Knipping, P. & Laue, M. Interferenzerscheinungen bei Röntgenstrahlen. *Ann. Phys. (Leipz.)* **346,** 971–988 (1913).
2. Madey, J. M. J. Stimulated emission of Bremsstrahlung in a periodic magnetic field. *J. Appl. Phys.* **42,** 1906–1913 (1971).
3. Huang, Z. & Kim, K.-J. Review of X-ray free-electron laser theory. *Phys. Rev. Spec. Top. Accel. Beams* **10,** 034801 (2007).
4. Galayda, J. N., Arthur, J., Ratner, D. F. & White, W. E. X-ray free-electron lasers—present and future capabilities [Invited]. *J. Opt. Soc. Am. B* **27,** B106–B118 (2010).
5. Emma, P. *et al.* First lasing and operation of an ångstrom-wavelength free-electron laser. *Nature Photon.* **4,** 641–647 (2010).
6. Bonifacio, R., Pellegrini, C. & Narducci, L. M. Collective instabilities and high-gain regime in a free electron laser. *Opt. Commun.* **50,** 373–378 (1984).
7. Ehrke, H. *et al.* Photoinduced melting of antiferromagnetic order in $La_{0.5}Sr_{1.5}MnO_4$ measured using ultrafast resonant soft X-ray diffraction. *Phys. Rev. Lett.* **106,** 217401 (2011).
8. Eichberger, M. *et al.* Snapshots of cooperative atomic motions in the optical suppression of charge density waves. *Nature* **468,** 799–802 (2010).
9. Kwon, O.-H. & Zewail, A. H. 4D electron tomography. *Science* **328,** 1668–1673 (2010).
10. Hoener, M. *et al.* Ultraintense X-ray induced ionization, dissociation, and frustrated absorption in molecular nitrogen. *Phys. Rev. Lett.* **104,** 253002 (2010).
11. Fang, L. *et al.* Double core-hole production in N_2: beating the auger clock. *Phys. Rev. Lett.* **105,** 083005 (2010).
12. Young, L. *et al.* Femtosecond electronic response of atoms to ultra-intense X-rays. *Nature* **466,** 56–61 (2010).
13. Kanter, E. P. *et al.* Unveiling and driving hidden resonances with high-fluence, high-intensity X-ray pulses. *Phys. Rev. Lett.* **107,** 233001 (2011).
14. Neutze, R., Wouts, R., van der Spoel, D., Weckert, E. & Hajdu, J. Potential for biomolecular imaging with femtosecond X-ray pulses. *Nature* **406,** 752–757 (2000).
15. Johansson, L. C. *et al.* Lipidic phase membrane protein serial femtosecond crystallography. *Nature Methods* **9,** 263–265 (2012).
16. Seibert, M. M. *et al.* Single mimivirus particles intercepted and imaged with an X-ray laser. *Nature* **470,** 78–81 (2011).
17. Ackermann, W. *et al.* Operation of a free-electron laser from the extreme ultraviolet to the water window. *Nature Photon.* **1,** 336–342 (2007).
18. Shintake, T. *et al.* A compact free-electron laser for generating coherent radiation in the extreme ultraviolet region. *Nature Photon.* **2,** 555–559 (2008).
19. Pile, D. X-rays: first light from SACLA. *Nature Photon.* **5,** 456–457 (2011).
20. Ding, Y. *et al.* Measurements and simulations of ultralow emittance and ultrashort electron beams in the Linac coherent light source. *Phys. Rev. Lett.* **102,** 254801 (2009).
21. Krinsky, S. & Gluckstern, R. Analysis of statistical correlations and intensity spiking in the self-amplified spontaneous-emission free-electron laser. *Phys. Rev. Spec. Top. Accel. Beams* **6,** 050701 (2003).
22. Düsterer, S. *et al.* Femtosecond X-ray pulse length characterization at the Linac Coherent Light Source free-electron laser. *New J. Phys.* **13,** 093024 (2011).
23. Ding, Y. *et al.* Femtosecond X-ray pulse temporal characterization in free-electron lasers using a transverse deflector. *Phys. Rev. Spec. Top. Accel. Beams* **14,** 120701 (2011).
24. Grguraš, I. *et al.* Ultrafast X-ray pulse characterization at free-electron lasers. *Nature Photon.* **6,** 852–857 (2012).

25. Frühling, U. *et al.* Single-shot terahertz-field-driven X-ray streak camera. *Nature Photon.* **3,** 523–528 (2009).
26. Itatani, J. *et al.* Attosecond streak camera. *Phys. Rev. Lett.* **88,** 173903 (2002).
27. Kienberger, R. *et al.* Atomic transient recorder. *Nature* **427,** 817–821 (2004).
28. Hentschel, M. *et al.* Attosecond metrology. *Nature* **414,** 509–513 (2001).
29. Kruit, P. & Read, F. H. Magnetic field paralleliser for 2π electron-spectrometer and electron-image magnifier. *J. Phys. E* **16,** 313–324 (1983).
30. Gagnon, J. & Yakovlev, V. S. The direct evaluation of attosecond chirp from a streaking measurement. *Appl. Phys. B* **103,** 303–309 (2011).
31. Drescher, M. *et al.* Time-resolved atomic inner-shell spectroscopy. *Nature* **419,** 803–807 (2002).
32. Schins, J. *et al.* Observation of laser-assisted Auger decay in argon. *Phys. Rev. Lett.* **73,** 2180–2183 (1994).
33. Glover, T., Schoenlein, R., Chin, A. & Shank, C. Observation of laser assisted photoelectric effect and femtosecond high order harmonic radiation. *Phys. Rev. Lett.* **76,** 2468–2471 (1996).
34. Gagnon, J. & Yakovlev, V. S. The robustness of attosecond streaking measurements. *Opt. Express* **17,** 17678–17693 (2009).
35. Glownia, J. M. *et al.* Time-resolved pump–probe experiments at the LCLS. *Opt. Express* **18,** 17620–17630 (2010).
36. Bozek, J. D. AMO instrumentation for the LCLS X-ray FEL. *Eur. Phys. J. Spec. Top.* **169,** 129–132 (2009).
37. Emma, P. *et al.* Femtosecond and subfemtosecond X-ray pulses from a self-amplified spontaneous-emission-based free-electron laser. *Phys. Rev. Lett.* **92,** 074801 (2004).

Acknowledgements

Portions of this research were carried out at the Linac Coherent Light Source (LCLS) at SLAC National Accelerator Laboratory. LCLS is an Office of Science User Facility operated for the US Department of Energy (DOE) Office of Science by Stanford University. The work was partly supported from the German cluster of excellence 'Munich-Centre for Advanced Photonics'. W.H., W.S. and R.K. acknowledge financial support by the BACATEC programme. W.H., A.R.M. and W.S. acknowledge 'The International Max Planck Research School on Advanced Photon Science' for funding and continued inspiring support. W.H. acknowledges financial support from a Marie Curie fellowship. A.R.M. thanks S. Reiche for fruitful discussions and help with GENESIS simulations. C.R. and G.D. acknowledge partial support from the US DOE (DE-FG02-04ER15614) and the National Science Foundation (NSF; PHY-1004778). G.D. also acknowledges support from US Department of Energy/Basic Energy Sciences (US DOE/BES; DE-AC02-06CH11357). J.T.C. acknowledges support from Science Foundation Ireland (grant no. 12/IA/1742). R.K. acknowledges funding from an European Research Council Starting Grant. The authors thank T. Schätz for comments on the manuscript. The authors thank P. Emma, Y. Ding, J.B. Hastings and W. White for their support, C. Behrens and H.-D. Nuhn for their expertise and advice on FEL-related questions, and to the whole scientific and technical team at LCLS for their dedication and unrelenting work during our beam time, in particular to the machine operators.

Author contributions

W.H. and A.R.M. contributed equally to the work. R.K. developed the concept. W.H., A.R.M., W.S., I.G., P.R., G.D., C.R., J.G., Ma.M., S.S., C.B., L.F.D., J.D.B., R.C., A.L.C. and R.K. designed the experiment and contributed to the preparation of the experimental set-up. W.H., A.R.M., W.S., I.G., P.R., G.D., C.R., Ma.M., S.S., C.B., D.C., J.D.B., Th.T., J.T.C., Mi.M., R.C., S.D., A.L.C. and R.K. performed the experiment. W.H., A.R.M., W.S., I.G., P.R., G.D., J.G., A.L.C. and R.K. analysed the data. W.H., A.R.M., G.D., J.G., F.G., L.F.D., Th.T., J.T.C., Mi.M., S.D., A.L.C. and R.K. wrote the paper.

Additional information

Supplementary information is available in the online version of the paper. Reprints and permissions information is available online at www.nature.com/reprints. Correspondence and requests for materials should be addressed to R.K.

Competing financial interests

The authors declare no competing financial interests.